JOURNAL OF GEOPHYSICAL RESEARCH, VOL 90, PAGES 12,121-12,132, DECEMBER 1, 1985

The Hidden Ion Population - Revisited

R. C. Olsen
Physics Department, The University of Alabama in Huntsville, Huntsville, AL 35899

C. R. Chappell, D. L. Gallagher, J. L. Green
Solar Terrestrial Physics Division, Space Science Laboratory, NASA/Marshall Space Flight Center, Huntsville, AL 35812

D. A. Gurnett
Department of Physics and Astronomy, University of Iowa

Satellite potentials in the outer plasmasphere range from near zero to +5 to +10 V. Under such conditions ion measurements may not include the low energy core of the plasma population. In eclipse, the photoelectron current drops to zero, and the spacecraft potential can drop to near zero volts. In regions where the ambient plasma density is below 100 cm^{-3}, previously unobserved portions of the ambient plasma distribution function can become visible in eclipse. A survey of the data obtained from the Retarding Ion Mass Spectrometer (RIMS) on Dynamics Explorer 1 shows that the RIMS detector generally measured the isotropic background in both sunlight and eclipse in the plasmasphere. Absolute density measurements for the "hidden" ion population are obtained for the first time using the Plasma Wave Instrument observations of the upper hybrid resonance. Agreement in total density is found in sunlight and eclipse measurements at densities above 80 cm^{-3}. In eclipse, agreement is found at densities as low as 20 cm^{-3}. The isotropic plasma composition is primarily H+, with ~10% He+, and 0.1 to 1.0% 0+. A low energy field-aligned ion population appears in eclipse measurements outside the plasmasphere, which is obscured in sunlight. These field-aligned ions can be interpreted as field-aligned flows with densities of a few particles per cm3, flowing at 5-20 km/s. The problem in measuring these field-aligned flows in sunlight is the masking of the high-energy tail of the field-aligned distribution by the isotropic background. Effective measurement of the core of the magnetospheric plasma distributions awaits satellites with active means of controlling the satellite potential.

1. INTRODUCTION

1.1. History

Plasma measurements in the magnetosphere should provide enough information to determine the plasma density, temperature, mass composition, and pitch angle distribution. Complementary particle and wave measurements of the plasma density have shown that at times there is good agreement between the two. *Gurnett and Frank* [1974] compared 88-eV to 38-keV particle measurements in the plasma sheet with the total electron density as determined from the lower cutoff frequency of continuum radiation, measured by the plasma wave instrument on Imp 6. GEOS-1 wave and plasma measurements in the plasmasphere showed good agreement when the spacecraft potential was low (0 to +2 V, density greater than 5 cm s). Outside the plasmasphere, at higher spacecraft potentials (+2 to +5 V), agreement was poorer, particularly with the ion detectors [*Decreau et al.,* 1978]. It was speculated that some part of the pitch angle distribution was not being observed, that an unsampled high-energy population might provide the difference, or that the cold plasma was excluded from the spacecraft ion detectors by the positive spacecraft potential. One clue that this last alternative was correct came from data taken in eclipse by the SCATHA satellite. Particle data taken with an electrostatic analyzer showed that a cold plasma population (T ~ 0.5 eV) with a density between 10 and 100 cm^{-3} appeared suddenly when the satellite was eclipsed, but was hidden in sunlight [*Olsen, 1982a*]. The analyzers used for these measurements had a sharp drop in sensitivity below 2 eV that left open the possibility that a different instrument might succeed in measuring the cold plasma distribution in sunlight as well as eclipse. Also, these measurements were not complemented by wave data, limiting the determination of absolute densities.

The purpose of this paper is to show further measurements of ordinarily 'hidden' ion populations, resolving some of the questions raised by the SCATHA data, reported by *Olsen* [1982a]. In particular, we will address the questions of absolute density, low energy sensitivity, and provide mass composition measurements of the 'hidden' ion population.

1.2 Spacecraft and Instruments

Dynamics Explorer 1 (DE-1) satellite was launched into a polar orbit on August 3, 1981, with a perigee of 675 km altitude, and an apogee of 4.65 RE. The 7.5-hour orbit began with apogee over the north pole, precessing to the equator (in the midnight sector) in the spring of 1982. The spacecraft spins in a reverse cartwheel fashion, at 10 rpm with its spin axis perpendicular to the orbit plane.

The Retarding Ion Mass Spectrometer (RIMS) is composed of 3 sensor assemblies. The radial sensor head views perpendicular to the spin axis and provides pitch angle distributions, while sensors on the ends of the spacecraft view along the spin axis to provide complete phase space coverage. The radial sensor head has an angular resolution of ±10°in the

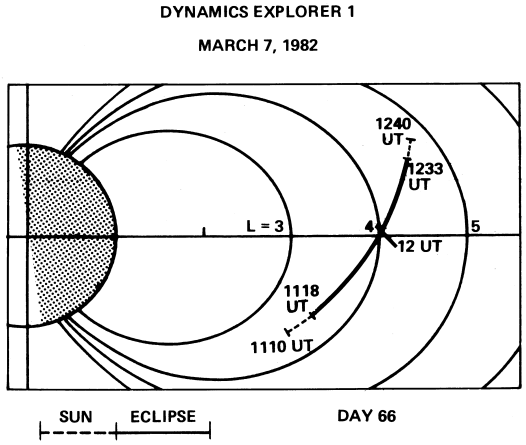

Figure 1. Orbit plot for March 7, 1982 (Day 66), the eclipse portion of the orbit segment is indicated by the solid orbit trace, from 1117-1230. Dashed lines indicate the sunlit portions of the orbit.

spin plane and ±55° perpendicular to the spin plane. The end heads, or Z heads, have roughly conical apertures with 55° half angles. Each instrument covers the 1-32 AMU mass range with two channels. The low channel covers the 1-8 AMU range, the high channel 4-32 AMU. In this paper, we will show H+ and He+ data using the low (1 AMU) and high (4 AMU) mass channels concurrently, and 0+ data from the high channel. A retarding potential analyzer (RPA) precedes the mass analysis segment of each instrument, with a voltage sweep from 0 to 50 V. An anomaly in the radial RPA in October, 1981, preceded the spring, 1982 eclipse season, precluding energy analysis of field-aligned ions. The geometric factor in H+ for the end heads is approximately 8.10^{-3} cm^2 ster. The accumulation period is 12 ms, and 50-100 measurements are typically summed over before creating a distribution function. [*Chappell et al., 1981*].

The plasma wave instrument (PWI) experiment provides wave information from 1.8 Hz up to 409 kHz, using a low frequency correlator (LFC) from 1.8 - 100 Hz, and step frequency receivers (SFR) from 104 Hz to 409 kHz. The SFR covers the 104 Hz to 409 kHz range in 128 steps. In the normal operational mode, a complete frequency sweep takes 32 s--just over 5 spins of the spacecraft. The data used in this paper come from the long electric antenna (200 m tip- to-tip) perpendicular to the spin axis (Ex) [*Shawhan et al., 1981*].

Magnetic field data are obtained from the DE-1 Goddard Space Flight Center magnetometer [Farthing et al., 1981]. These data provide the gyrofrequency and pitch angle information needed to interpret the wave frequency spectra and particle angular distributions.

2. OBSERVATIONS

Observations from GEOS and SCATHA [Decreau et al., 1978; Olsen, 1982a] show that the typical floating potential for a satellite in the outer plasmasphere is between +2 and +10V. In eclipse, the spacecraft potential would drop to a negative potential of the order of the electron thermal energy (ti0.5 eV), if it were not for secondary emission. With 100-1000 eV electrons present, i.e., at the inner edge of the plasma sheet, it is possible to have a floating potential in eclipse of up to +5V [*Olsen, 1982a*]. As the cold electron flux increases with respect to the warm electron flux, the potential should drop.

We begin with data taken deep in the plasmasphere, where the spacecraft potential in sunlight is only a few tenths of a volt. Next, data taken near the plasmapause (densities just below 100 cm 3) are shown, illustrating the 1 volt shift in potential found there. The remaining illustrations focus on the outer plasmasphere (or plasmapause) regions, with densities below 100 cm s, and anisotropic plasma distributions. These latter cases are primarily field-aligned plasmas suggestive of ion flows into the plasmasphere, i.e., refilling.

2.1 Plasmasphere observations-isotropic plasma

Data from DE-1 taken on March 7, 1982, illustrate changes in the RIMS data caused by small variations in spacecraft potential. Figure 1 shows the orbit segment presented next. The satellite enters eclipse at L = 3.4, 1118 UT, and exits eclipse at L = 4.6, 1233 UT. The satellite crosses the magnetic equator at 1200 UT. Plate 1 shows the RIMS and PWI data prior to, during, and following the eclipse. The top panel shows the 10-400 kHz portion of the plasma wave data, which includes the upper hybrid resonance (UHR). The UHR shows a monotonic drop over the period illustrated, reflecting the increase in "L" for the outbound satellite. Of particular note is the lack of change in the plasma wave data at the eclipse transitions. The wave data provide a control on measuring possible environmental changes occurring at the same time as eclipse transition. The remaining panels show the hydrogen and helium RPA analysis for the end head (90° pitch angle) data, and the spin distribution for the helium and oxygen. The spin-time plots are ordered such that the center line corresponds to 'ram' data, i.e., data taken along the satellite's direction of motion. The pitch angles are indicated by the white lines across the panel, giving the spin phases for the minimum and maximum pitch angles (usually 0° and 180°). The oxygen and helium spin distribution peaks along the ram direction, indicating isotropic plasma distributions. Substantial changes in the helium flux are apparent at the eclipse transition. The end head (perpendicular to **B** and the ram vector) show a substantial drop in flux at eclipse exit for H+ and He+.

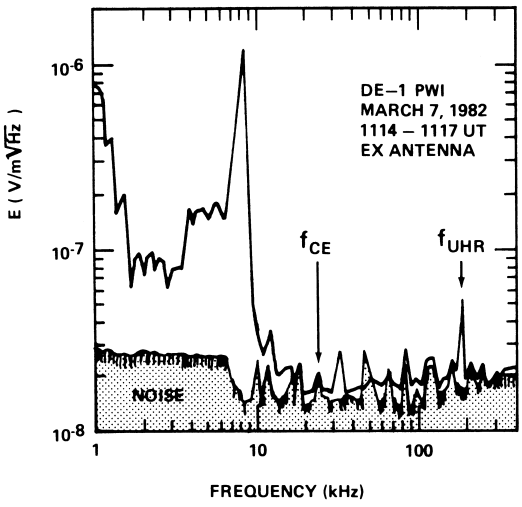

Figure 2. Electric field measurements from the Plasma Wave Instrument (PWI) show the upper hybrid resonance (UHR), which is used to establish the total electron density. The electron gyrofrequency (f_{ce}) is also identified.

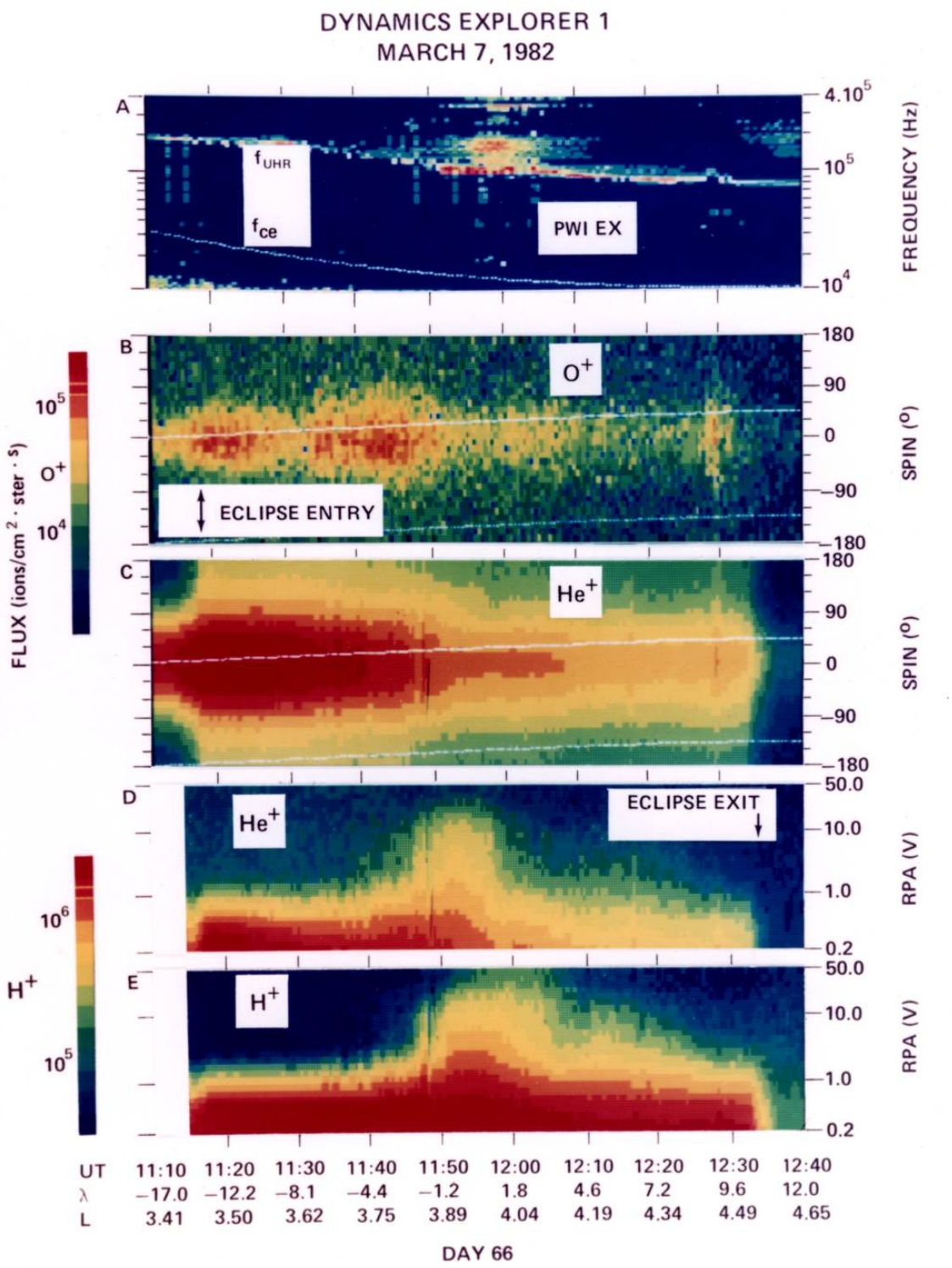

Plate 1. A) Plasma wave data. The dotted white line is the electron gyrofrequency. The main signal visible here is the upper hybrid resonance (UHR), beginning at 200 kHz at 1110 UT and dropping monotonically to 80 kHz at 1240 UT. B) Oxygen spin-time spectrogram. The dashed white line near the center is the minimum pitch angle locus. C) Helium spin-time spectrogram. The flux scale is close to that shown for hydrogen. D) Helium RPA-time spectrogram. E) Hydrogen RPA-time spectrogram. The peak in flux exceeding 10 V on the RPA scale, from 1150 to 1200 UT is due to the equator crossing and plasmapause density gradient.

Figure 2 shows the plasma wave data at eclipse entry. The upper hybrid resonance gives a total electron density of 420 cm s. The Retarding Potential Analyzer (RPA) curves from one of the end heads (-Z) at eclipse entry are shown as distribution functions in Figures 3a and 3b for hydrogen and helium, respectively. There is a shift in the detector assembly potentials of about half a volt, between partial sunlight (1115) and total eclipse (1119). There is no clear indication of a negative potential in eclipse. This detector assembly typically appears to be a few tenths of a volt higher in potential than the radial detector (shown next). The sum of the hydrogen and helium densities is equal to the electron density, to within the uncertainties in the calibration of the end heads.

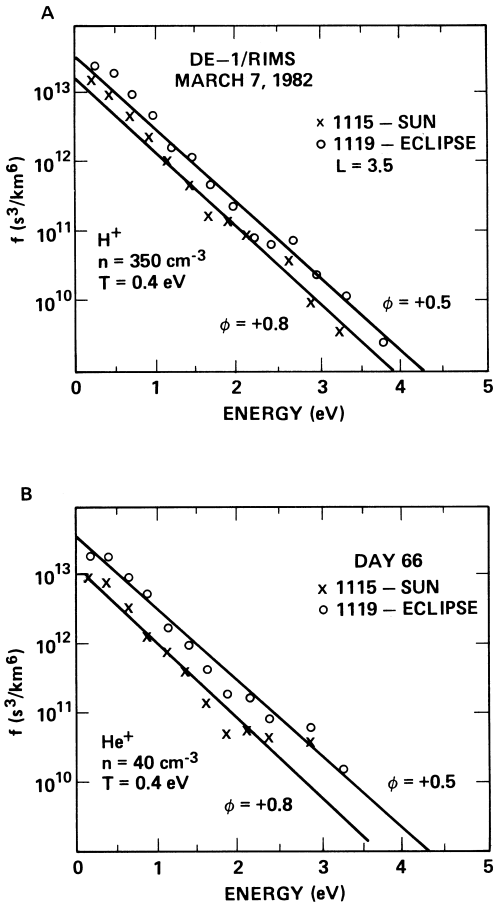

Figure 3. Ion distribution functions for (a) hydrogen and (b) helium are shown for eclipse (1119 UT), and partial sunlight (1115 UT). The satellite potential shifted a few tenths of a volt over this period.

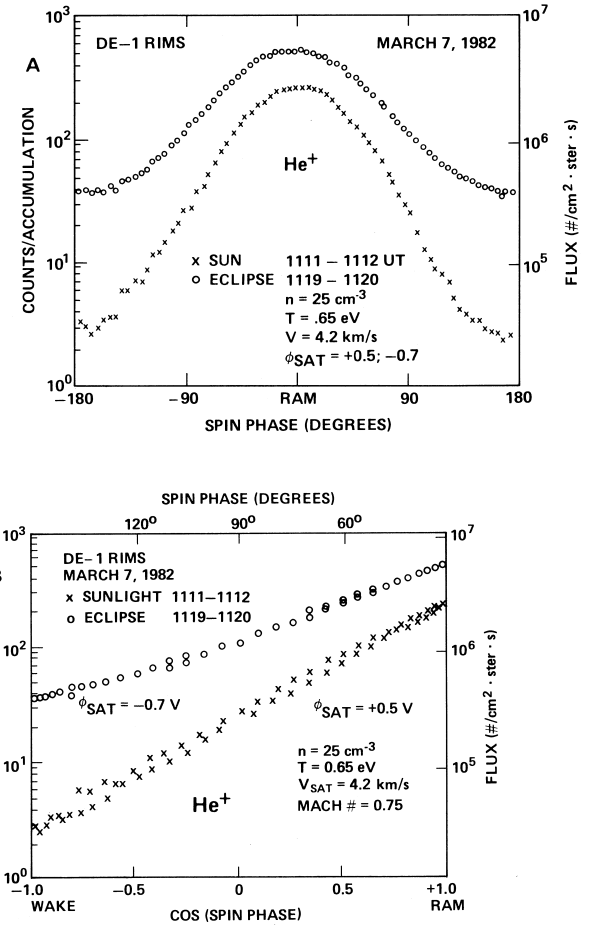

Figure 4. Helium fluxes are shown as a function of spin phase for eclipse (1119 UT) and sunlight (1111 UT). Data are plotted versus (a) the spin phase and (b) the cosine of the spin phase. There is a shift in potential of over a volt due to the eclipse.

The hydrogen and helium show the same temperature, an extremely useful feature of the plasmasphere, recently noted by *Comfort et al.* [1985]. This equal temperature feature can frequently be used to aid the analysis process, particularly when analyzing spin curves. The two masses give Mach numbers which vary by a factor of 4 for rammed plasmas. This can aid in determining a unique value for the detector potential.

Figures 4a and 4b show the helium spin curves for sunlight and eclipse. (The hydrogen channeltron is severely degraded at this time, and is not used). Analysis of the spin curves is based upon the numerical simulation of an RPA response after equation (19) in *Whipple et al*. [1974].

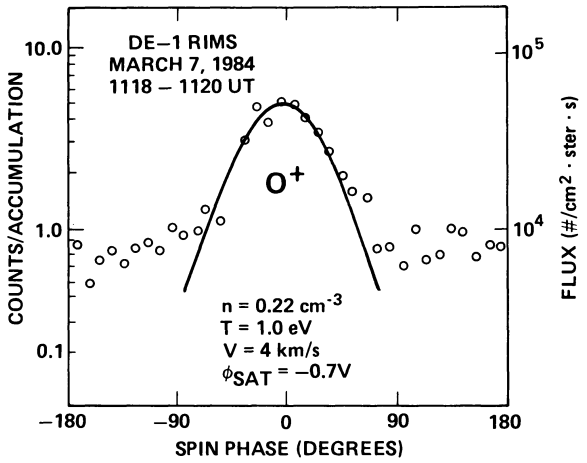

Figure 5. Oxygen data from eclipse are shown plotted vs. spin phase. Each data point represents an average of several hundred accumulation intervals (12 ms interval).

An example of the numerical simulation of a RIMS spin curve is shown by *Comfort et al*. [1985]. The fits shown here are based on analytical expressions resulting from fits to a large ensemble of numerical simulations [R. H. Comfort, private communication, 1985]. Figure 4a shows a traditional plot versus the angle of attack, or ram angle. The second version (Figure 4b) shows the data plotted versus the cosine of the ram angle. This choice of ordinate orders the data as a nearly straight line, with the slope of the line depending on the Mach number (and hence temperature) in much the same way the plots of distribution function versus energy do. Figure 4b shows how the slope of the curve also depends upon spacecraft potential, growing steeper as the potential rises. These data illustrate the behavior of the mass spectrometer when it is measuring all of the ambient plasma in sunlight as well as eclipse. The oxygen measurements made by the radial detector are shown in Figure 5. Oxygen is a minor ion at this time, with a density which is about 1% of the helium density, and a temperature which is higher than that of the light ions, H+ and He+. Due to the high ram energy of the oxygen (> 1 eV), there is little effect on the oxygen data caused by the small shift in detector potential at eclipse entry. These measurements are typical of the midnight region oxygen data. Oxygen typically has a temperature 50% to 100% higher than the light ions, reflecting different source and transport characteristics.

The satellite exits eclipse an hour later. The plasma density has dropped to 80 cm^{-3}, as indicated by the plasma wave data in Figure 6. The RPA sweeps have again been converted into distribution functions, and it is apparent that the ambient hydrogen is measured in sunlight and eclipse, as shown in Figure 7. The peak hydrogen count rate is quite low in sunlight, less than ten counts per accumulation. The helium count rate in sunlight is down to the background level (less than one count per accumulation). This appears to be an analog to the electrostatic analyzer measurements on ATS6 and SCATHA reported by *Olsen* [1982a]. The helium distribution is present, but the end head only measures it in eclipse. The hydrogen fluxes are low enough to be missed by any detector which fails to go below 1 eV, or is less sensitive than the RIMS detector. In eclipse, the sum of the hydrogen and helium densities is again equal to the total electron density inferred from the PWI measurements.

This combination of detector and satellite has an advantage over an electrostatic analyzer on a geosynchronous satellite. The detector looking in the direction of the satellite velocity not only gains from the kinetic energy of the ram plasma, but there is an effective focusing of the plasma, i.e., the plasma is "scooped up". This is illustrated by the helium spin curves obtained during the eclipse exit period (Figure 8). There are only 5 or 6 counts per accumulation in the ram direction in sunlight, but a recognizable spin curve still persists. The same plasma parameters can be used to fit both the eclipse and sunlight data shown in Figure 8, by varying the detector potential by 2.5 V.

2.2 Field-Aligned Plasma Observations

Observations of anisotropic plasmas are also affected by the change in spacecraft potential caused by variations in photoemission. Field-aligned flows, such as the polar wind, are expected to have kinetic energies of 1 to 2 eV. Such plasmas have been observed over the polar cap with DE-1/ RIMS [*Nagai et al*., 1984, RC Olsen et al, unpublished manuscript]. The spacecraft potential at such times was +3 to +4 V, and it was necessary to bias the experiment package negative with respect to the satellite to measure polar wind plasma. Near-equatorial measurements made in eclipse provide an opportunity to measure such flows without resorting to aperture bias techniques. Examples will be shown from two days. The first shows field-aligned plasmas which will be interpreted as flows along the magnetic field at 5-7 km/s, with the second eclipse data set suggesting field-aligned flow velocities 2 to 10 times higher.

February 28, 1982 Figure 9 shows the orbital segment for the second eclipse example. The plasmapause indicated at L = 3.6, 0820 UT, is based on the observed 100 cm^{-3} boundary and the outer boundary of the cold isotropic plasma. The satellite entered eclipse near the magnetic equator, while inside the plasmasphere, at 0810 UT. The satellite exits eclipse outside the plasma-sphere, at 0930 UT. The plasma data are summarized in Plate 2. The UHR found in the top panel decreases monotonically from 400 kHz to 40 kHz over the eclipse period. The spin curves for H+, He+, and 0+ all show a transition from ram plasma (cold isotropic) to a mixture of isotropic and field-aligned plasma around 0820, as the satellite exits the plasmasphere. The RPA data from the end head show the warm temperatures typically found at the equator (0810), and a warm background plasma at later times, particularly in hydrogen.

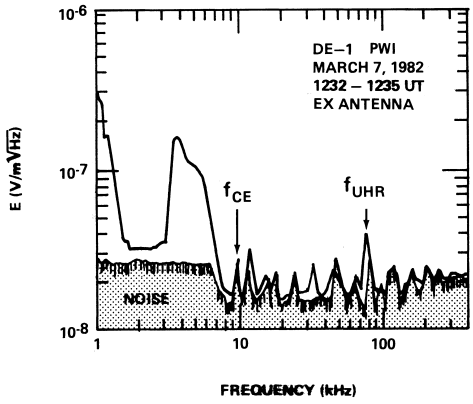

Figure 6. PWI measurements at eclipse exit.

Data are shown for two time segments, in eclipse at 0918-0920 UT, L = 4.4, λ_m= 22°; and at eclipse exit at 0930 UT, L = 4.5, λ_m = 24°. Figure 10 shows the PWI line spectra for the first of these two time segments (0918-0920). The UHR at 47 kHz gives a total electron density of 26 cm^{-3}. Figure 11 shows the RPA measurements (converted to distribution function) and Figure 12 shows the spin curves for measurements for this time. DE-1 is outside the plasmasphere, in a region of mixed plasma populations. The isotropic background is best illustrated by Figure 11, which shows the RPA data from the end head for the plasma at 90° pitch angle. A cold (T < 1 eV) plasma is found in the 0-5 eV energy range. A density of 17 cm^{-3} is inferred, so the isotropic component forms the largest part of the total ion density. The spin curves shown in Figure 12 show doubly peaked distributions are found for both hydrogen and helium. The center (ram) portion of these curves is filled in by the rammed, isotropic plasma.

Additional analysis of the spin curves (Figure 12) requires some assumptions about the nature of the field-aligned plasma. If this plasma is a flowing Maxwellian, then the Mach curve analysis used for isotropic plasmas is suitable. If these measurements are of a plasma which was isotropic at lower altitudes, and has simply folded in pitch angle with increasing altitude, then the Mach curve analysis is invalid.

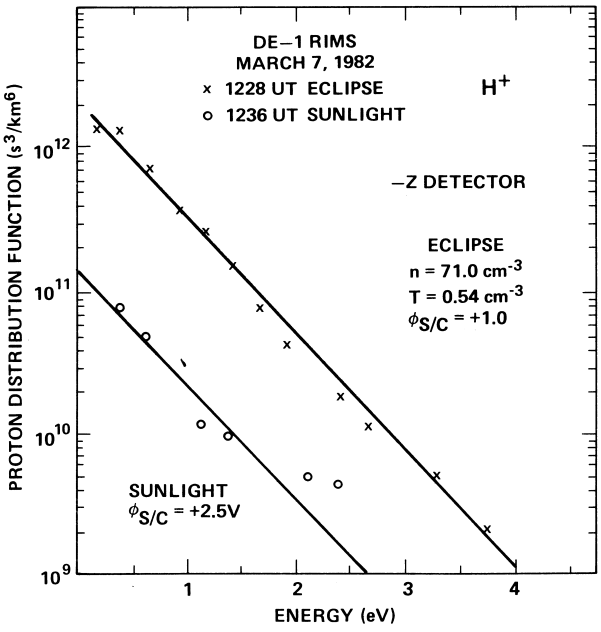

Figure 7. Ion distribution functions for hydrogen show a shift in detector potential of over 1 volt as the satellite exits eclipse.

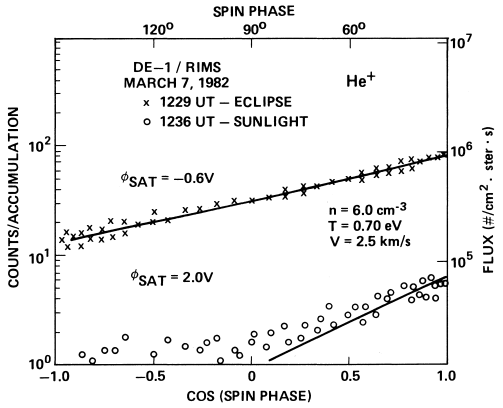

Figure 8. Helium spin curves for eclipse exit show a 2 to 3 V shift in the radial detector potential.

In the absence of a clear indication as to which case is appropriate, we proceed with the assumption that the field-aligned ions can be interpreted as a flowing Maxwellian. The first clue as to the flow velocity can be obtained from the angular offsets from the field line and ram direction. The spin curves shown in Plate 2 can be seen to peak at angles between the field-aligned direction (the white lines) and the ram direction (0° spin phase). When combined with the known spacecraft velocity, simple geometry provides a unique value for the flow velocity, if there are no E x B drifts. Such drifts will not be large at these altitudes (1-2 km/s), but are comparable to the satellite velocity (2.5 km/s) and hence could be important. For now, we assume

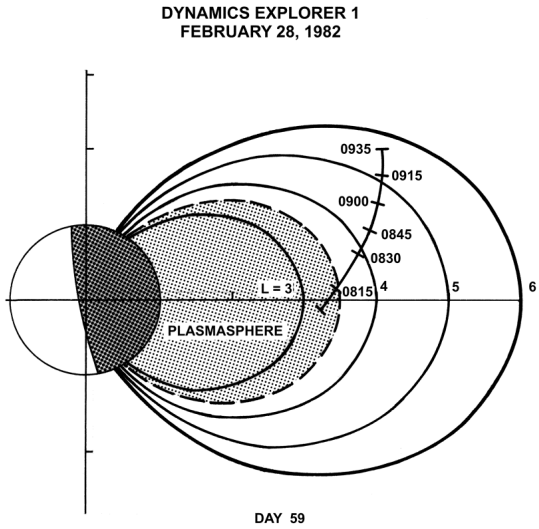

Figure 9. Orbit plot for February 28, 1982 (day 59). Figure 10. PWI measurements in eclipse.

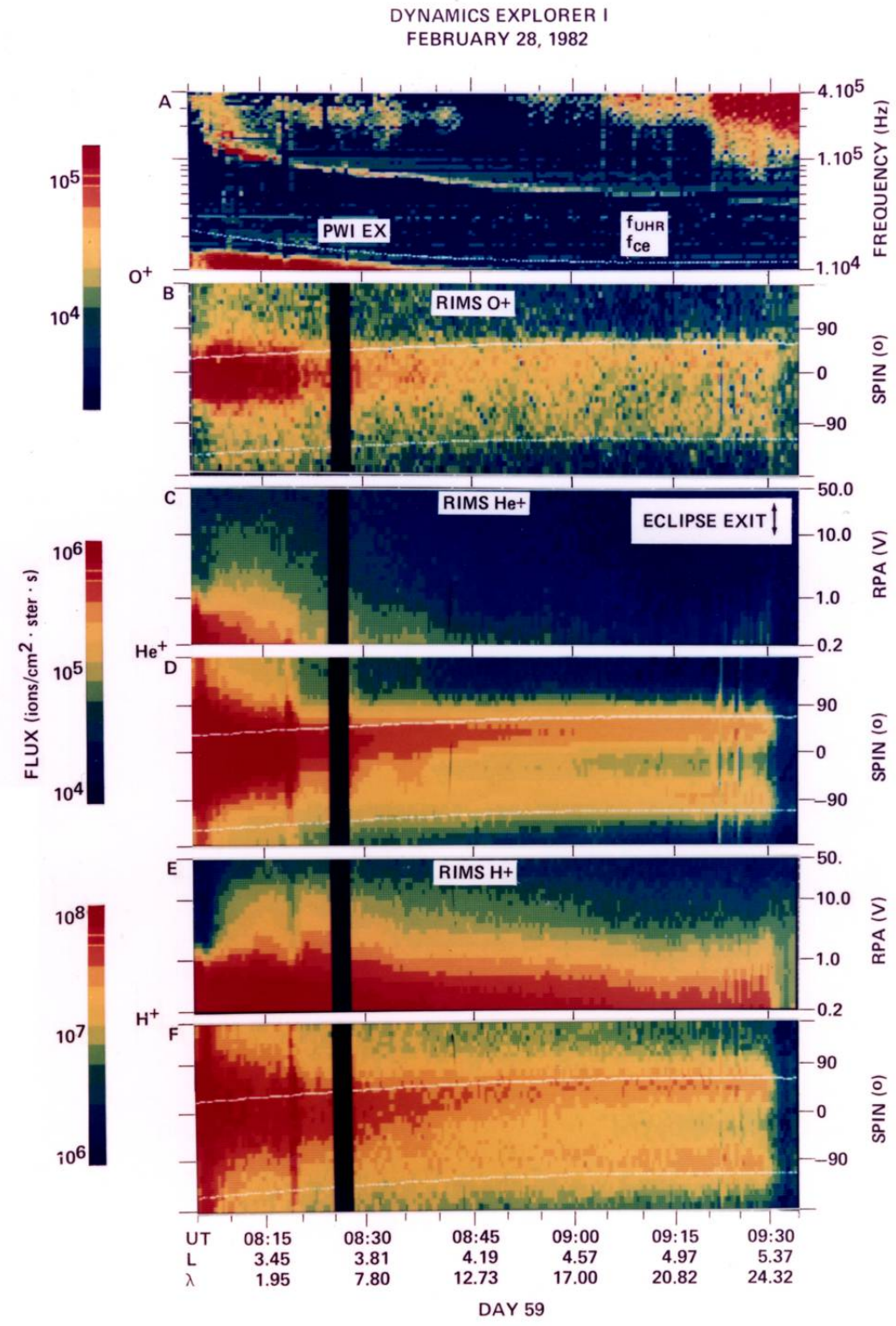

Plate 2. A) Plasma wave data. B) Oxygen spin-time spectrogram. C) Helium RPA-time spectrogram. D) Helium spin-time spectrogram. E) Hydrogen RPA-time spectrogram. F) Hydrogen spin-time spectrogram. The color bar count rate scales are for the radial detector, spin-time spectrograms.

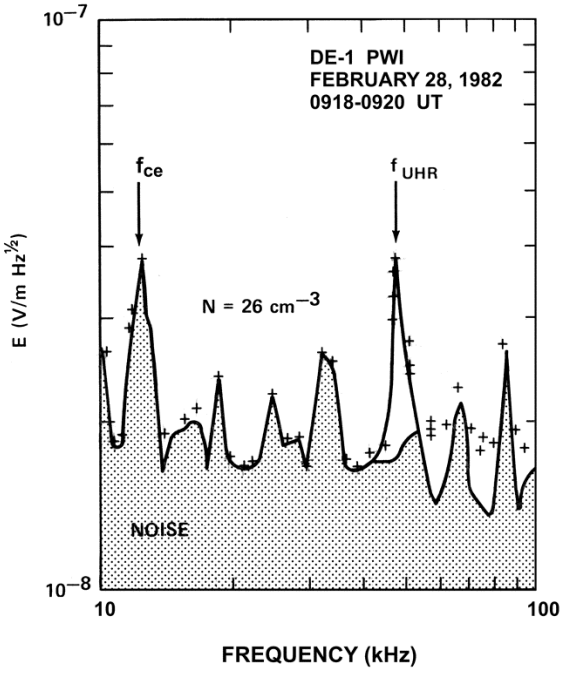

Figure 10. PWI measurements in eclipse.

there are no convection drifts, and simply sum the inferred field-aligned velocity with the satellite velocity to create the spin curves which overlay the data shown in Figure 12. The peaks in the hydrogen flux occur at spin phases of -92° and 57° or pitch angles of 22° and 168°. These offsets give field-aligned flow velocities of 6.5 and 11 km/s respectively. The peaks in the helium flux occur at spin phases of -87° and 48°, or pitch angles of 26° and 160°. The resulting field-aligned flow velocities are

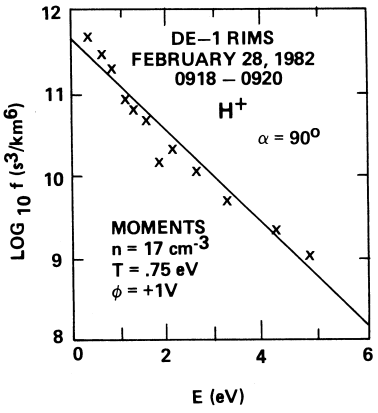

Figure 11. Distribution function for the isotropic hydrogen distribution measured during eclipse. The moments of the observed distribution function were used to construct an equivalent Maxwellian distribution, which overlays the data.

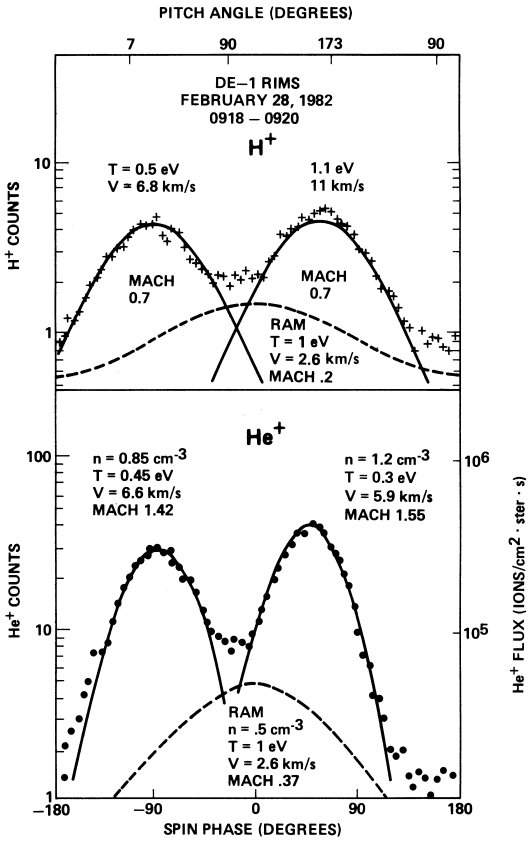

Figure 12. Spin curves for hydrogen and helium are shown with superimposed curves, based on the assumption that the observations are the sum of bi-directional field-aligned flows and the isotropic (ram) plasma observed by the -Z detector (Figure 10). Note that the velocity used in the fit to the data is the geometric sum of the satellite and field-aligned flow velocities. The hydrogen channeltron is severely degraded at this time; the hydrogen flux is nominally 100 times greater than the helium flux.

6.1 and 5.5 km/s. The satellite velocity is 2.56 km/s. Fitting the curves in Figure 12 with an assumed spacecraft potential of 0 V results in subsonic fits to the hydrogen, and supersonic fits to the helium curves. Temperatures are around half an electron volt. The inferred plasma parameters suggest that these may be ionospheric flows which may have lost some field-aligned flow energy to thermal energy. The difference between the RAM (0° spin phase) and WAKE (180° spin phase) data can be explained with the isotropic background as shown by the dashed curve.

Ten minutes later, at 0930 UT, the satellite exits eclipse. There have been some changes in the nature of the field-aligned plasma, and a small drop in the background density down to 23 m73 as inferred from PWI. Figure 13 shows the end head RPA data in eclipse and sunlight, and suggests a minimum shift in potential of 1.5 V as the cold portion of the plasma distributions disappears from the detectors view. Figure 14 shows the field-aligned plasma measurements. The hydrogen data (Figure 14a) are shown for eclipse only, since the count rate drops to the

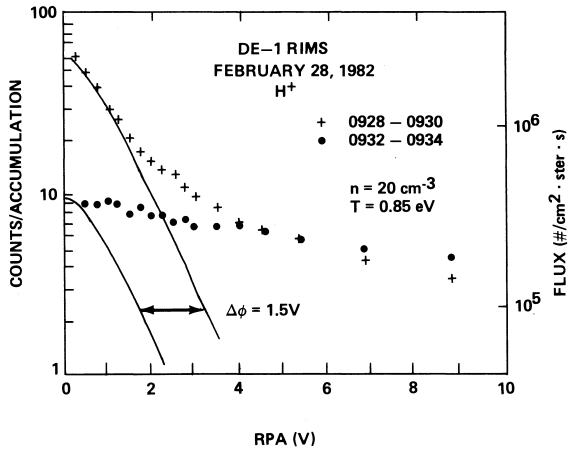

Figure 13. Hydrogen data from eclipse and sunlight show an increase in detector potential of 1.5 V or more as the satellite exits eclipse.

detector back-ground (0.4 counts/accumulation at this time) in sunlight. The helium flux (Figure 14b) also drops, though the field-aligned portion of the helium curve survives even in sunlight. The peaks in the hydrogen flux are at spin phases of -94° and 56°, or pitch angles 21° and 167°, resulting in field-aligned flow velocities of 7 and 11 km/s. The helium peaks are at spin phases of -91° and 45°, pitch angles 24° and 157°, with flow velocities 6 and 4 km/s. Both flows are supersonic. The satellite velocity is 2.46 km/s. The sunlight helium peaks shift 1° or 2°, indicating that spacecraft potential effects on the inferred flow directions are minimal. A shift in spacecraft potential of about 2 V brings the fits to the eclipse data in line with the sunlight data.

Figure 13 shows the isotropic background is lost when the ambient H+ plasma density is near 20 cm s, with sunlight potentials of 2 V or more. At best, the isotropic component might be measured in the radial detector on days when the channeltron is not degraded, but by comparison with the helium data, it appears that this component would not be detectable, with only the field-aligned plasma observed in sunlight.

February 21, 1982 The third example of eclipse plasma measurements is from February 21, 1982. Figure 15 shows the orbital segment presented next. Eclipse is from 0500 to 0610 UT. The plasmapause is crossed near L = 4.5, at 0530 UT. The satellite crosses the magnetic equator just prior to eclipse entry. Plate 3 shows the wave and thermal plasma data for this eclipse period. The spin distribution for H+, He+, and 0+ show ram plasma until 0530, a transition region of mixed plasmas, followed by a region of field-aligned distributions. The H RPA analyses (Panel E) shows the effect of a temperature gradient (high to low) from 0450 to 0515, reflecting the motion away from the magnetic equator (a region of warmer plasma). Cold plasma (T ≈ 0.5 eV) is seen in the RPA from 0515-0530. From 0530-0535 there is a mixture of cold, plasmasphere ions with the warmer (several eV) plasma of the inner plasmasheet. The warm background persists until just after eclipse exit. At that point the combination of increased satellite potential and possible environmental changes eliminate most of the low energy plasma from the RIMS view.

Concentrating on the later segment, higher flow velocities are inferred in our second example of anisotropic plasmas. The satellite leaves the plasmasphere at L = 4.4, as marked by the transition from isotropic plasma to field-aligned plasma, and the ambient electron density drops below 50 cm^{-3}. The plasma is field-aligned from L = 5 to 6. In the region of field-aligned ions (0540-0615 UT), the plasma wave data (top panel of Plate 3) show a feature near 20 kHz, between the electron gyrofrequency (f_{ce}) and the first harmonic. This may be the UHR, and can be traced back to the UHR prior to 0545. It is also possible that the signal is the 3/2 f_{ce} gyroharmonic. If it is the former, a density of 3 to 5 cm^{-3} can be inferred. Figures 16 and 17 show the spin curves for hydrogen and helium measured near L = 6.0 in eclipse and sunlight. The satellite is 30 degrees north of the magnetic equator. Hydrogen and helium both show doubly peaked distributions, with higher fluxes coming from the southern pole, through the equator. In sunlight, the hydrogen flux from the northern hemisphere drops by a factor of 25, with the flux from the south dropping to the level of the isotropic background (not instrumental background). The helium flux completely disappears, dropping to a background level of 0.2 counts/accumulation (2×10^3 ions/cm^2 sr s). The plasma wave data suggest that there are environmental changes occurring at eclipse exit which may explain some of these variations.

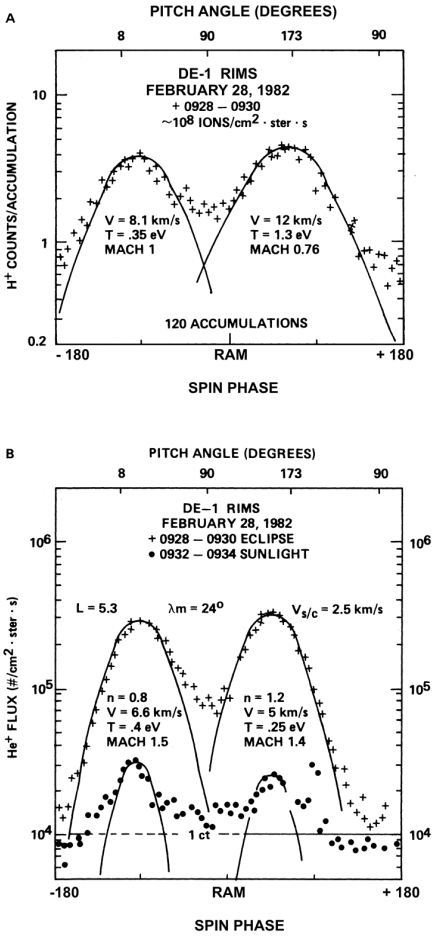

Figure 14. Spin curves for (a) hydrogen and (b) helium are shown for eclipse and sunlight. Eclipse measurements were fitted assuming zero detector potential.

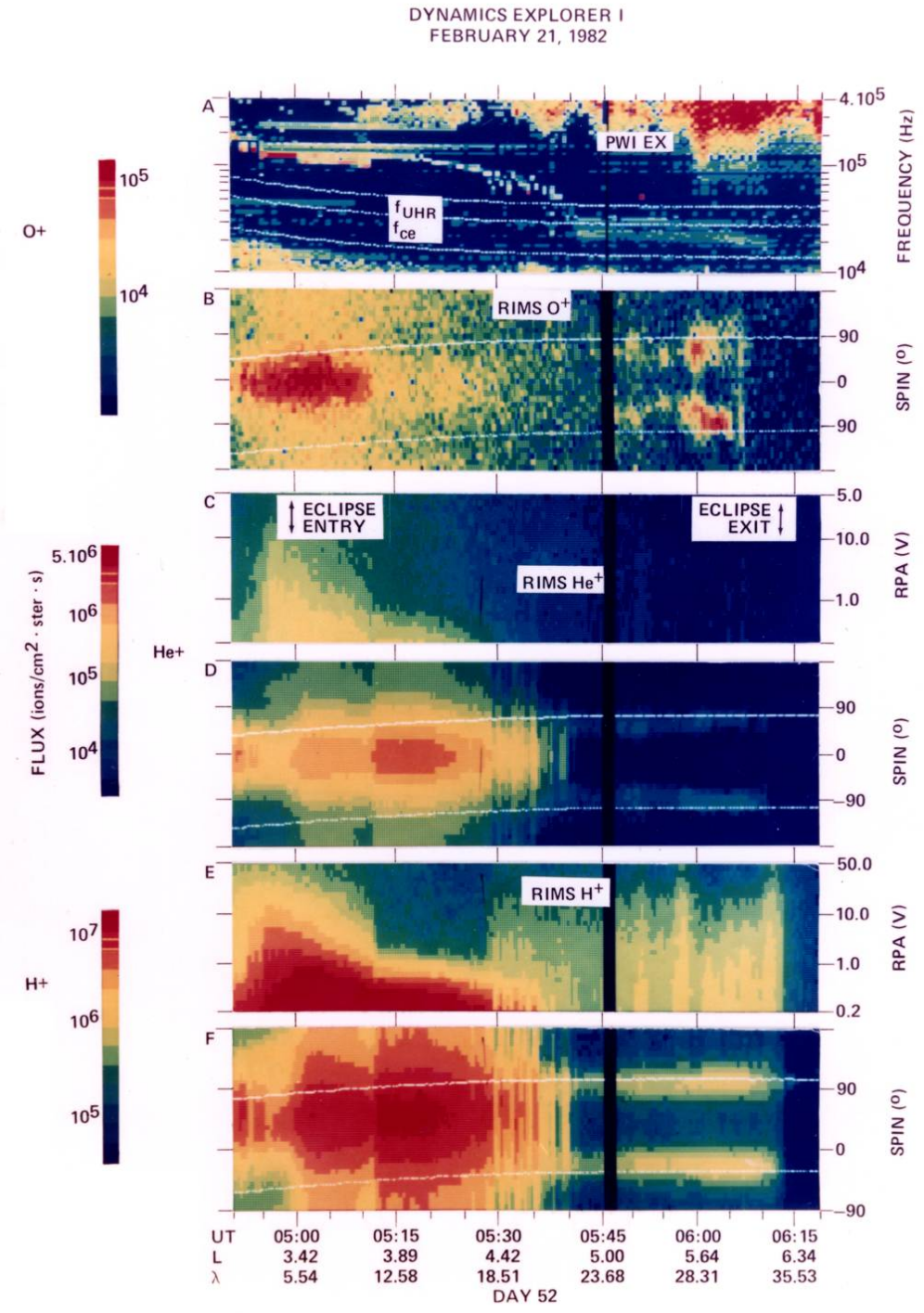

Plate 3. Same format as Plate 2

.

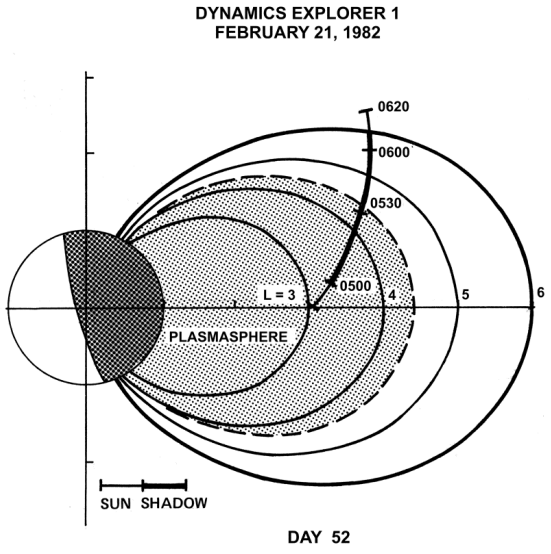

Figure 15. Orbit plot for February 21, 1982 (Day 52).

Apparently, the flow from the north is more energetic than the flow through the equator, and the shift in spacecraft potential masks only the flow from one direction (this is supported by the Mach curve analysis, discussed below for Figure 17). The persistence of the higher energy flow is reminiscent of the data obtained from ATS6, where field-aligned flow measurements near the inner edge of the plasmasheet could be made in sunlight, but were enhanced in eclipse [see Figures 4-6 of *Olsen*, 1982b].

Figure 17 shows the eclipse data with the flux plotted versus the cosine of the offset from the peak flux direction. For the flow from the southern hemisphere, the 6° offset from the field-aligned direction gives a velocity of 25 km/s, while the flow from the north (2° offset) gives 75 km/s. If there is a 2 km/s convection flow (a 1 mV/m field) the inferred parallel velocities drop to 6 and 17 km/s, respectively. These latter numbers represent probable lower bounds for the field-aligned velocities, since a near-equatorial electric field of a millivolt per meter would be a relatively large field, at local midnight, at L = 6. Fitting Mach curves to the angular distributions for spacecraft potentials of 0 and +5 V, and flow velocities of 15 and 30 km/s, results in temperatures between 0.5 and 1 eV, and densities of a few ions per cubic centimeter. These numbers are similar to those found at L = 6.6 with ATS-6, during quiet times at the inner edge of the plasma sheet [*Olsen*, 1982b)]

Energy analysis of the isotropic component (90° pitch angle) (not shown) reveals a warm (5 eV) background plasma with a density about 1 cm^{-3}. The satellite potential apparently increases by 5 to 10 V as the satellite exits eclipse, and the count rate drops below one count per accumulation, effectively preventing measurement of the background.

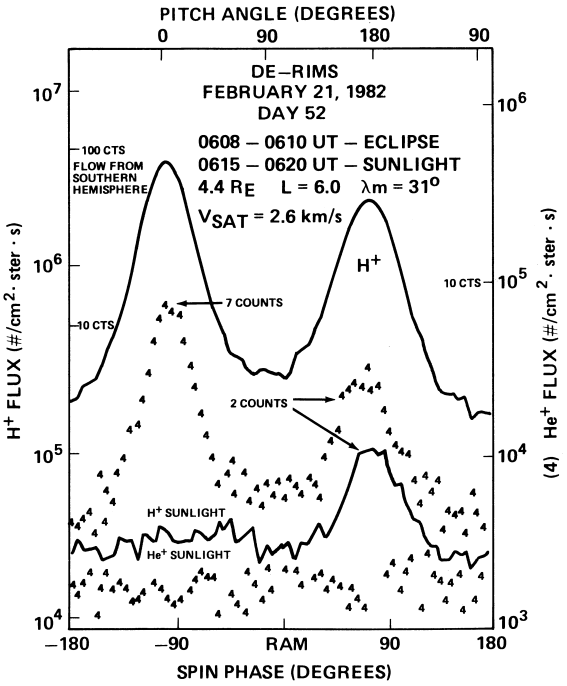

Figure 16. Spin curves for hydrogen (solid lines) and Helium (4) in eclipse and sunlight.

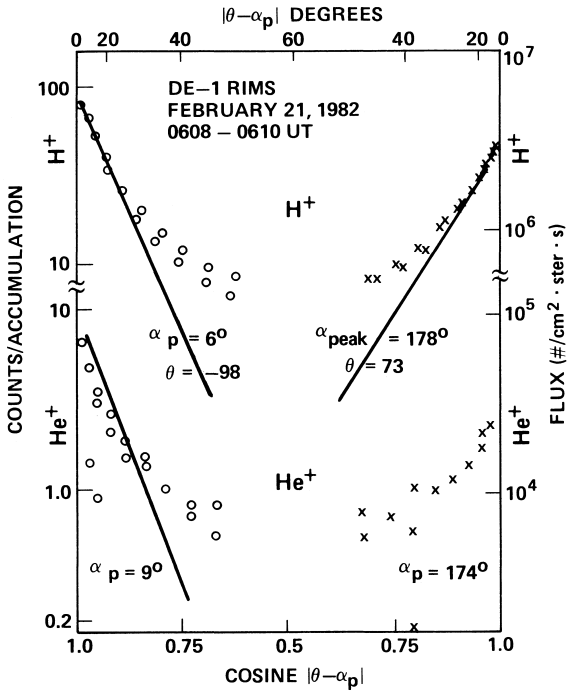

Figure 17. Spin curves for hydrogen and helium in eclipse, plotted against the cosine of the angle offset from the peak flux. Fits are made assuming a flowing Maxwellian, at zero volt detector potential.

3. SUMMARY

The data taken in the plasmasphere show the RIMS detector is capable of measuring the core of the plasma distribution in sunlight and eclipse, though the task is more easily done in eclipse. Isotropic plasma can be measured in sunlight or eclipse at densities greater than or equal to 100 $.m^{-3}$. As the satellite leaves the plasmasphere, and the potential of the satellite rises, the isotropic background can be lost. Isotropic plasma at the 20 cm^{-3} level is measured in eclipse, but not in sunlight with the detector looking away from the satellite direction of motion. Field-aligned flows can generally be measured in sunlight and eclipse, because of their high Mach numbers, but inferring plasma parameters is substantially easier in eclipse. If there is a large (+5 to +10 V) potential in sunlight, the low energy portion of the distribution is lost. If there is an isotropic background, it can obscure the remaining, higher energy portion of the field-aligned distribution (i.e. the tail of the distribution). The RIMS detector is more effective at measuring the core of the ambient plasma distribution than the electrostatic analyzers from ATS6 and SCATHA, but still can be said to be limited in its ability to measure all the plasma, all the time. Continuous effective measurements of the "hidden" ion population of the magnetosphere still awaits satellites with effective means of potential control. One method for doing so is to use a hollow cathode plasma source [*Olsen*, 1981]

ACKNOWLEDGEMENTS The authors would like to express their gratitude to the Data Systems Technology Program and Space Physics Analysis (SPAN) pilot project for providing access to computer and networking facilities. Special thanks go to M. Sugiura for use of his magnetic field data in the determination of the particle pitch angles. The research at The University of Alabama in Huntsville was supported by NASA contract NAS8-33982 and NSF grant ATM8-300426, and at the University of Iowa through contract NAS5-25690. The authors are indebted to the engineering and science staff of the University of Texas at Dallas and to the RIMS team at Marshall Space Flight Center. We are grateful to the programming staff of the Intergraph and Boeing Corporations for assistance with the data reduction software.

The Editor thanks E. C. Whipple and D. Winningham for their assistance in evaluating this paper.

REFERENCES

Chappell, C. R., J. L. Green, J. F. E. Johnson, and J. H. Waite, Pitch angle variations in magnetospheric thermal plasma-initial observations from Dynamics Explorer 1, *Geophys. Res. Lett.* 9, 933-936, 1982.

Chappell, C. R., S. A. Fields, C. R. Baugher, J. H. Hoffman, W. B. Hanson, W. W. Wright, and H. D. Hammack, The retarding ion mass spectrometer on Dynamics Explorer-A, *Space Sci. Inst.*, 5, 477-491, 1981.

Comfort, R. H., C. R. Baugher, and C. R. Chappell, Use of the thin sheath approximation for obtaining ion temperatures from the ISEE-1 limited aperture RPA, *J. Geophys. Res.*, 87, 5109,1982.

Comfort, R. H., J. H. Waite, and C. R. Chappell, Thermal ion temperatures from the Retarding Ion Mass Spectrometer on DE 1, *J. Geophys. Res.*, 90, 3475-3486, 1985.

Decreau, P. M. E., J. Etcheto, K. Knott, A. Pedersenm G. L. Wrenn, and D. T. Young, Multi-experiment determination of plasma density and temperature, *Space Sci. Rev.*, 22, 633-645, 1978.

Farthing, W. H., M. Sugiura, B. G. Ledley, and L. J. Cahill, Magnetic Field Observations on DE-A and -B, *Space Sci. Inst.*, 5, 551-560, 1981.

Green, J. L. D. A. Gurnett, and S. D. Shawhan, The angular distribution of auroral kilometric radiation, *J. Geophys. Res.*, 82, 1825 - 1838, 1977.

Gurnett, P. A. and L. A. Frank, Thermal and suprathermal plasma densities in the outer magnetosphere, *J. Geophys. Res.*, 79, 2255-2361, 1974.

Nagai, T., J. H. Waite, J. L. Green, C. R. Chappell, R. C. Olsen, R. H. Comfort, First measurements of the supersonic polar wind in the polar magnetosphere, *Geophys. Res. Lett.,* 11, 669-672, 1984.

Olsen, R. C., Modification of spacecraft potentials by plasma emission, *J. Spacecraft Rockets*, 18, 462-469, 1981.

Olsen, R. C., The hidden ion population of the magnetosphere, *J. Geophys. Res.*, 87, 3481-3488, 1982a.

Olsen, R. C., Field-aligned ion streams in the earth's midnight region, *J. Geophys. Res.*, 87, 2301-2310, 1982b.

Olsen, R. C., C. E. Mcllwain, and E. C. Whipple, Observations of differential charging effects on ATS-6, *J. Geophys. Res.*, 86, 6809-6819, 1981.

Olsen, R. C., C. R. Chappell, and J. L. Burch, Aperture plane potential control for thermal plasma measurements, submitted to JGR, 1985.

Shawhan, S. D., D. A. Gurnett, D. L. Odem, R. A. Helliwell, and C. G. Park, The plasma wave and quasi-static electric field instrument (PWI) for Dynamics Explorer-A, *Space Sci. Inst.*, 5, 535-550, 1981.

Singh, N., and C. R. Baugher, Sheath effects on current collection by particle detectors with narrow acceptance angles, *Space Sci. Instrum.*, 5, 295-305, 1981.

Sojka, J. J., R. W. Shunk, J. F. E. Johnson, J. H. Waite, and C. R. Chappell, Characteristics of thermal and suprathermal ions associated with the dayside plasma trough as measured by the Dynamics Explorer Retarding Ion Mass Spectrometer, *J. Geophys. Res.*, 88, 7895-7911, 1983.

Whipple, E. C., J. M. Warnock, and R. W. Winckler, Effect of satellite potential on direct ion density measurements through the plasmapause, *J. Geophys. Res.,* 79, 179-186, 1974.

Received December 26, 1984;
revised May 27, 1985;
accepted May 21, 1985.)